Supporting Information

Manuscript title: Satisfactory Anti-Interference and High Performance of 1Co-1Ce/Mn@ZSM-5 Catalyst for Simultaneous Removal of NO and Hg^0 in Abominable Flue Gas

Authors: Huawei Zhang, Zishun Li, Ting Liu*, Mingzhu Zhang, Shengnan Deng, Yincui Li, Peng Liang

Number of pages: 21

Number of Tables: 3

Number of Figures: 7

Preparation of 1Co-1Ce/Mn@ZSM-5 Catalyst. The exhaust gas was treated with potassium permanganate solution, sodium hydroxide solution and activated carbon before being discharged into the atmosphere. In addition, in order to ensure the quality of the experimental data, all experiments were repeated 3 times. The Mn@ZSM-5 molecular sieve was synthesized by hydrothermal method, and then the active component of Co-CeO_x was loaded by impregnation method, which was named *x*Co-1Ce/Mn@ZSM-5. Firstly, 8.30g of tetrapropyl ammonium hydroxide and 0.821g of sodium aluminate were stirred with water as depicted in **Figure S1**, when it was clarified it would be moved into water bath with 60°C. Then TEOS and ethanol were added for stirring for 3 h, and the mixture was recorded as solution A. Secondly, a certain amount of $MnSO_4$ and $KMnO_4$(molar ratio of 8:3) were stirred with water for 30 min according to the loading capacity of 2 wt% Mn, which was recorded as solution B. Thirdly, the solution A was put into solution B, in which 5ml ethylene glycol was added and stirred at 60°C for 3 h. Fourthly, the obtained solution was transferred to the high pressure reaction kettle and reacted for 72 h at 180°C. The procedures of washing, drying and burning immediately followed at 550°C for 4h. Finally, ion exchange was performed at room temperature and repeated three times. The sample is named Mn@ZSM-5. As a contrast, ZSM-5 zeolite was also obtained by using the similar approach without adding of $MnSO_4$ and $KMnO_4$.

A certain amount of $Ce(NO_3)_2 \cdot 6H_2O$ and $Co(NO_3)_2 \cdot 6H_2O$ with three different Co/Ce mole ratios ($x_{(Co/Ce)}$=0.5, 1.0, and 2.0, respectively) were dissolved in 40 mL distilled water for ultrasonic dispersion for 15 min. Subsequently, 2.0 g of Mn@ZSM-

5 sample was mixed to the resultant solutions and stirred for 3.5 h at room temperature, and then the resulting product was filtered, dried at 80°C overnight and calcined at 500°C for 3 h. Lastly, the sample was vacuumized at 150°C and then ultrasonically dispersed into 10 mL anhydrous toluene at room temperature, and then a certain amount of cetyltrimethoxy silane was added and stirred for 24 h at room temperature. After stirring the mixture was filtered, washed with ethanol, and dried overnight at 100°C to obtain the final *x*Co-1Ce/Mn@ZSM-5. The spent samples are named Mn@ZSM-5-SH and 1Co-1Ce/Mn@ZSM-5-SH.

Characterization of Catalyst. As listed in **Table S1**, the BET surface area of ZSM-5 zeolite is 360.843 m^2/g, the total pore volume is 0.206 cm^3/g, and the average pore size is 0.411 nm. When the Mn nanoparticles are loaded on ZSM-5, the specific surface area of Mn@ZSM-5 catalyst is similar to that of ZSM-5 zeolite, and it can be observed that the pore sizes of the samples are 0.41 nm and 0.45 nm respectively. Meanwhile, the micropore volume matches well, except that the average pore size increases by 0.448 nm, indicating that the Mn is well dispersed in the skeleton or on the surface of the material, which is consistent with the BET results in **Table S1**, and part of Mn is doped into the skeleton of ZSM-5 molecular sieve, increasing the pore size slightly. The typical morphology of the prepared Mn@ZSM-5 molecular sieve in **Figure S2a-2b** is the stacking of small diamond-shaped crystals with grain size 100-300nm. The crystal lattice of MnO_2 is obvious, corresponding to the crystal plane of (002), and the lattice spacing is 0.726 nm. In the TEM image of 1Co-1Ce/Mn@ZSM-5 sample (**Figure S2e**), it could be clearly observed that the lattice spacing of points (1), (2) and (3) are 0.726

nm, 0.311 nm and 0.495 nm, which is corresponded to the (002), (111) and (311) crystal planes of MnO_2, CeO_2 and Co_3O_4, respectively.

The ZSM-5 and Mn@ZSM-5 samples in **Figure S3** show a type I nitrogen adsorption curve, which is in accordance with the typical microporous structure accompanying with the sharp rise in the low-pressure section (P/P_0) and no obvious hysteresis loop in the high-pressure section (P/P_0) [1]. Differently, the adsorption and desorption isotherms of the 1Co-1Ce/Mn@ZSM-5 catalyst not only have obvious absorption at the low-pressure stage P/P_0, but also show a hysteresis loop shape at the middle pressure stage P/P_0[2]. The possible reason is that the organsilyl ation treatment of 1Co-1Ce/Mn@ZSM-5 catalyst maintains the zeolite skeleton structure and forms open mesoporous, which is confirmed by the new pore size distribution at 3.0-5.0 nm. As shown in **Figure S5**, compared to the pure zeolite, all the peaks match the standard phase of ZSM-5 zeolite, whereas for manganese containing materials slight shifting to smaller angle is observed. It means that parts of manganese oxides entered the framework of the zeolite during crystal formation, resulting in an increase in the value of lattice parameters.

It is believed that the high Mn^{4+} and O_α content on the surface of 1Co-1Ce/Mn@ZSM-5 catalyst promote the catalytic reaction of NH_3-SCR and Hg^0 oxidation at low temperature[3, 4]. The conversion between Ce^{4+} and Ce^{3+} on the surface of 1Co-1Ce/Mn@ZSM-5 catalyst enables CeO_2 to store and release oxygen and attributes to the excellent catalytic oxidation. In addition, Co^{3+} could produce anion

defects and reduce the activation energy of NO chemisorption, which is conducive to rapid SCR reaction[5]. Therefore, proper amount of Co and Ce doping on Mn@ZSM-5 can effectively improve the removal performance of NO and Hg^0.

The H_2-TPR spectra of Mn@ZSM-5 and 1Co-1Ce/Mn@ZSM-5 catalysts are shown in **Figure S4**. Compared with Mn@ZSM-5, the reduction peak from intermediate to MnO in 1Co-1Ce/Mn@ZSM-5 catalyst is slightly deviated to low temperature due to the doping of Co and Ce. In addition, the reduction peak of 1Co-1Ce/Mn@ZSM-5 catalyst increase with the decrease of reduction temperature. Moreover, the reduction peak area of 1Co-1Ce/Mn@ZSM-5 is larger than Mn@ZSM-5, indicating that the 1Co-1Ce/Mn@ZSM-5 catalyst has an excellent catalytic reduction performance on the removal of NO and Hg^0.

Figure S5 showed the XRD patterns of fresh sample ZSM-5, Mn@ZSM-5 and 1Co-1Ce/Mn@ZSM-5 catalysts. It could be seen from the **Figure S5a** that the synthesized ZSM-5 zeolite crystallizes well, and its typical diffraction peaks are located at 7.83°, 8.73°, 22.99°, 23.83° and 24.34°, indicating that all samples have all characteristic diffraction peaks of standard ZSM-5 zeolite crystal[6, 7]. For Mn@ZSM-5 sample, typical diffraction peaks at 12.26°, 55.99° and 32.95° appeared in XRD, corresponding to crystal plane of MnO_2 (002), MnO_2 (301) and Mn_2O_3 (222), which is in good agreement with TEM results. Compared with Mn@ZSM-5, the presence of CeO_2 and Co_3O_4 at 28.71° and 35.90° correspond to the (111) and (311) crystal faces,

indicating that the Co and Ce nanoparticles are successfully supported on the ZSM-5 zeolite.

Anti-SO_2 Mechanism in the Presence of H_2O. The XRD patterns of Mn@ZSM-5-SH and 1Co-1Ce/Mn@ZSM-5-SH samples, which is obtained with the flue gas containing 500ppm SO_2 and 5vol% H_2O for 6h, are shown in the **Figure S7**. For the Mn@ZSM-5-SH catalyst, the (112) and (311) crystal faces of $MnSO_4$ appeared at 33.06° and 55.25°, indicating that in the presence of SO_2 the catalyst produces crystalline sulfate groups, which is the key factor for the catalytic deactivation of NO and Hg^0. In the 1Co-1Ce/Mn@ZSM-5-SH sample, a $CoSO_4$ diffraction peak appears at 34.69° corresponds to the (301) crystal plane. No diffraction peak of cerium sulfate is discovered, and it is speculated that the element Co prevents the SO_2 poisoning of Mn and Ce active sites. Thus, the sulfur tolerance of 1Co-1Ce/Mn@ZSM-5-SH sample is more superior to the Mn@ZSM-5-SH.

Figure S7 shows that the XPS spectra of Mn 2p, Co 2p, Ce 3d and O 1s of Mn@ZSM-5 and 1Co-1Ce/Mn@ZSM-5 samples, and the calculated atomic relative concentrations are shown in the **Table S2**. The Mn 2p spectrum in **Figure S7a** could be fitted by three peaks located at 640.4eV, 641.9eV and 643.5eV, which are classified as Mn^{2+}, Mn^{3+}, and Mn^{4+}, respectively[8]. The Co 2p spectrum in **Figure S7b** consists of seven peaks, which can be decomposed into two spin-orbit double peaks, D1 and D2, and three satellite peaks, S1, S2 and S3. The bimodal positions of D1 (780.6-781.1 eV and 795.0-795.9 eV) are Co^{3+}, and the bimodal positions of D2 (782.2-782.6 eV and 797.1-797.7 eV) are Co^{2+}[9, 10]. Typically, the Ce 3d spectrum in **Figure S7c** consists of

eight peaks, in which the double peaks of u/v, u''/v'' and u'''/v''' can be matched to Ce^{4+}, and the double peaks of u'/v' correspond to Ce^{3+}[11, 12].Therefore, the presence of Ce^{3+} and Ce^{4+} promotes the chemical redox cycle of the catalyst. The O 1s spectrum in **Figure S7d** can be fitted by two peaks of chemisorbed oxygen (O_α) and lattice oxygen (O_β). The peak position of 531.8eV belongs to O_α, and the peak position of 530.4eV belongsto O_β. As can be seen from the calculation results in the **Table S2**, the relative contents of Mn^{4+} and O_α increase by 13.49% and 12.61% after Co and Ce doping.

For Mn@ZSM-5 catalyst in **Figure S7a**, there are two reduction peaks at 343.4°C and 501.8°C, which may be related to the reduction of MnO_2 to MnO with Mn_2O_3 and Mn_3O_4 as intermediate[13]. The 1Co-1Ce/Mn@ZSM-5 catalyst has two large peaks in the temperature range of 200-900°C, and six small peaks could be synthesized by Gaussian curve fitting method. Among them, two reduction peaks appear at 344°C and 450°C, corresponding to the reduction of MnO_2 to Mn_2O_3/Mn_3O_4 and Mn_3O_4 to MnO[14]. The peaks center at 412°C and 527°C are ascribed to the reduction of chemisorbed oxygen, and the small peak at 748°C is due to the reduction of lattice oxygen in CeO_2[15]. The weak reduction peak at low temperature of 385°C corresponds to the reduction of Co_3O_4[16].

REFERENCE

[1] Dey, K. P.; Ghosh, S.; Naskar, M. K. Organic template-free synthesis of ZSM-5 zeolite particles using rice husk ash as silica source. Ceram. Int. 2014, *39* (2), 2153-2157;

[2] Luo, X.; Guo, J.; Chang, P.; Qian, H.; Pei, F.; Wang, W.; Miao, K.; Guo, S.; Feng, G. ZSM-5@MCM-41 composite porous materials with a core-shell structure: Adjustment of mesoporous orientation basing on interfacial electrostatic interactions and their application in selective aromatics transport. Sep. Purif. Technol. 2020, *239*, 116516;

[3] Zhong, J.; Zeng, Y.; Zhang, M.; Feng, W.; Xiao, D.; Wu, J.; Chen, P.; Fu, M.; Ye, D. Toluene oxidation process and proper mechanism over Co_3O_4 nanotubes: Investigation through in-situ DRIFTS combined with PTR-TOF-MS and quasi in-situ XPS. Chem. Eng. J. 2020, *397*, 125375;

[4] Wang, C.; Zhang, C.; Hua, W.; Guo, Y.; Lu, G.; Gil, S.; Giroir-Fendler, A. Catalytic oxidation of vinyl chloride emissions over Co-Ce composite oxide catalysts. Chem. Eng. J. 2017, *315*, 392-402;

[5] Machocki, A.; Ioannides, T.; Stasinska, B.; Gac, W.; Avgouropoulos, G.; Delimaris, D.; Grzegorczyk, W.; Pasieczna, S. Manganese-lanthanum oxides modified with silver for the catalytic combustion of methane. Journal of Catalysis 2004, *227* (2), 282-296;

[6] Kim, H. S.; Park, N. K.; Lee, T. J.; Urn, M. H.; Kang, M. Preparation of Nanosized-Particles Using a Microwave Pretreatment at Mild Temperature. Adv. Mater. Sci. Eng. 2012, *2012* (11);

[7] Feng, B.; Song, C.; Gang, L.; Song, J.; Wu, S.; Li, X. Selective catalytic reduction of nitric oxide with ammonia over zirconium-doped copper/ZSM-5 catalysts. Appl. Catal. B: Environ. 2014, *s 150–151* (1), 532-543;

[8] Zhang; D.; L.; Shi; Fang; C.; Li; H.; Gao; R. In situ supported MnOx-CeOx on carbon nanotubes for the low-temperature selective catalytic reduction of NO with NH_3. Nanoscale 2013;

[9] Hu, H.; Cai, S.; Li, H.; Huang, L.; Shi, L.; Zhang, D. Mechanistic Aspects of deNOx Processing over TiO_2 Supported Co-Mn Oxide Catalysts: Structure-Activity Relationships and In Situ DRIFTs Analysis. ACS Catal. 2015;

[10] Serrano-Lotina, A.; Iglesias-Juez, A.; Monte, M.; Vila, P. MnO_2-supported catalytic bodies for selective reduction of NO with NH_3: Influence of NO_2 and H_2O. Mol. Catal. 2020, *491*, 111004;

[11] Chen, L.; Wang, X.; Cong, Q.; Ma, H.; Li, S.; Li, W. Design of a hierarchical Fe-ZSM-5@CeO_2 catalyst and the enhanced performances for the selective catalytic reduction of NO with NH_3. Chem. Eng. J. 2019, *369*, 957-967;

[12] Lei; Zhang; Dengsong; Jianping; Sixiang; Cai; Cheng; Fang; Huang; Hongrui. Design of meso-TiO_2@MnO(x)-CeO(x)/CNTs with a core-shell structure as DeNO(x) catalysts: promotion of activity, stability and SO_2-tolerance. Nanoscale 2013, *5* (20), 9821-9829;

[13] Wang, X.; Xie, Y. C. The promotion effects of Ba on manganese oxide for CH_4 deep oxidation. Catal. Let. 2001, *72* (1), 51-57;

[14] Liu, Y.; Zhang, P. Catalytic decomposition of gaseous ozone over todorokite-type manganese dioxides at room temperature: Effects of cerium modification. Appl. Catal. B: Environ. 2016, *530*, 102-110;

[15] Zhang, H.; Ke, Z.; Gao, Y.; Tian, Y.; Peng, L. Inhibitory effects of water vapor on elemental mercury removal performance over cerium-oxide-modified semi-coke. Chem. Eng. J. 2017, *324*;

[16] Zhang, X.; Shen, Q.; He, C.; Ma, C.; Cheng, J.; Liu, Z.; Hao, Z. Decomposition of nitrous oxide over Co-zeolite catalysts: role of zeolite structure and active site. Catal. Sci. Technol. 2012, *2* (6), 1249-1258;

Table captions:

Table S1. The BET parameters of the contrasted samples.

Table S2. Relative concentrations of Mn, O, Co, and Ce in the fresh catalysts.

Table S3. Relative concentrations of Mn, O, Co, and Ce in the spent catalysts.

Table S1. The BET parameters of the contrasted samples.

Sample	Specific surface area (m^2/g)	Total volume capacity (cm^3/g)	Average pore size (nm)
ZSM-5	360.843	0.206	0.411
Mn@ZSM-5	359.226	0.205	0.448
1Co-1Ce/Mn@ZSM-5	291.961	0.188	0.653

Table S2. Relative concentration of Mn, O, Co, and Ce in the fresh catalysts.

Catalyst	Mn2p(%)			Co2p(%)		Ce3d(%)		O1s(%)	
	Mn^{2+}	Mn^{3+}	Mn^{4+}	Co^{2+}	Co^{3+}	Ce^{3+}	Ce^{4+}	O_{α}	O_{β}
Mn@ZSM-5	9.32	51.17	39.51	-	-	-	-	64.49	35.51
1Co-1Ce/Mn@ZSM-5	8.54	38.47	52.99	20.28	79.72	14.56	85.44	73.72	26.28

Table S3. Relative concentrations of Mn, O, Co, and Ce in the spent catalysts.

(%)		Mn@ZSM-5-SH	1Co-1Ce/Mn@ZSM-5-SH
Mn2p	Mn^{2+}	24.66	16.39
	Mn^{3+}	45.01	35.32
	Mn^{4+}	30.33	48.29
Co2p	Co^{2+}	-	31.18
	Co^{3+}	-	68.82
Ce3d	Ce^{3+}	-	19.23
	Ce^{4+}	-	80.77
O1s	$O_{\alpha}+O_{\gamma}$	65.30	82.29
	O_{β}	34.70	17.70
N1s	NH_4^+	49.64	53.73
	C-N	50.36	46.27
S2p	SO_3^{2-}	34.93	54.30
	SO_4^{2-}	65.07	45.50

Figure captions:

Figure S1. The procedure of sample preparation.

Figure S2. SEM of Mn@ZSM-5 sample(a, b); SEM and HRTEM of Mn@ZSM-5(c, d); HRTEM of 1Co-1Ce/Mn@ZSM-5(e).

Figure S3. CO_2 adsorption/desorption isotherm (a) and pore size distribution of the samples (b).

Figure S4. H_2-TPR spectra of different catalysts.

Figure S5. XRD patterns of different catalysts (a) and (b). (—ZSM-5; —Mn@ZSM-5; —1Co-1Ce/Mn@ZSM-5).

Figure S6. XPS spectra of different catalysts (a: Mn2p; b: O1s; c: Co2p; d: Ce3d).

Figure S7. XRD spectra of spent Mn@ZSM-5-SH and 1Co-1Ce/Mn@ZSM-5-SH catalysts (500ppm SO_2 and 5vol% H_2O for 6 h).

Figure S1. The procedure of sample preparation.

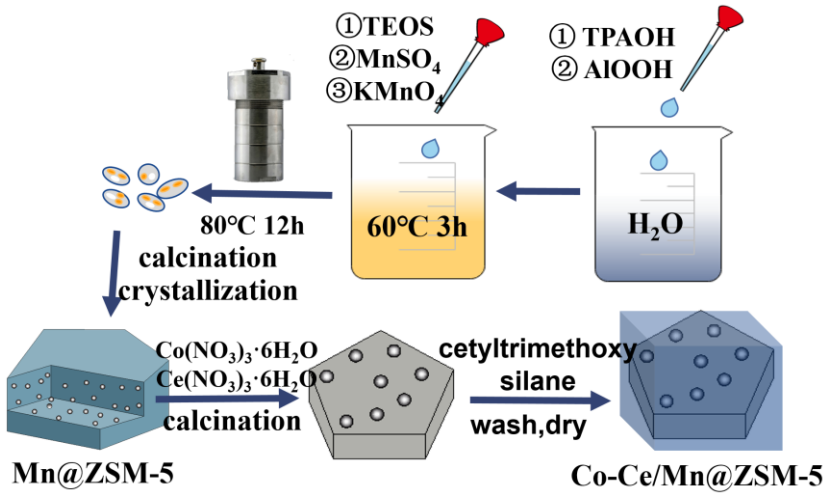

Figure S2. SEM of Mn@ZSM-5 sample(a, b); SEM and HRTEM of Mn@ZSM-5 (c, d); HRTEM of 1Co-1Ce/Mn@ZSM-5 (e).

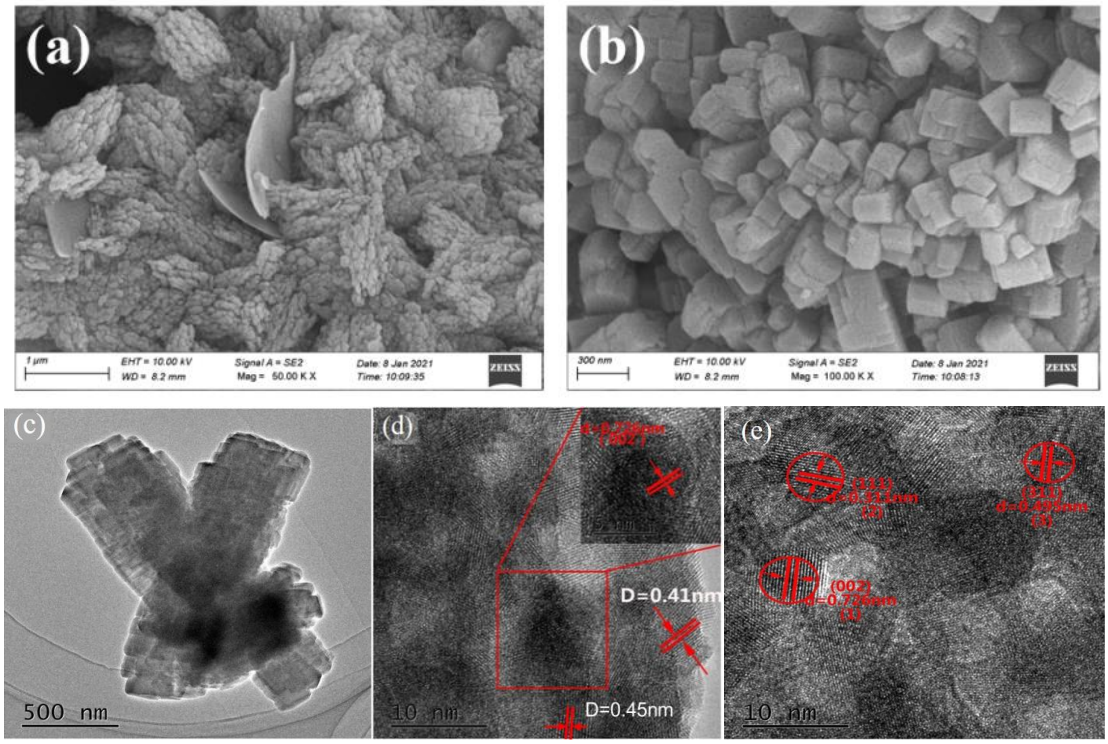

Figure S3. CO_2 adsorption/desorption isotherm (a) and pore size distribution of the samples (b).

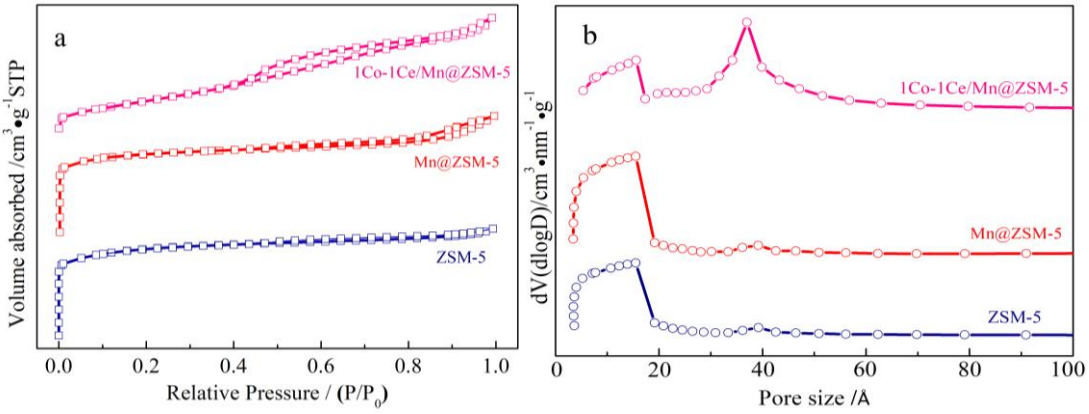

Figure S4. H_2-TPR spectra of different catalysts.

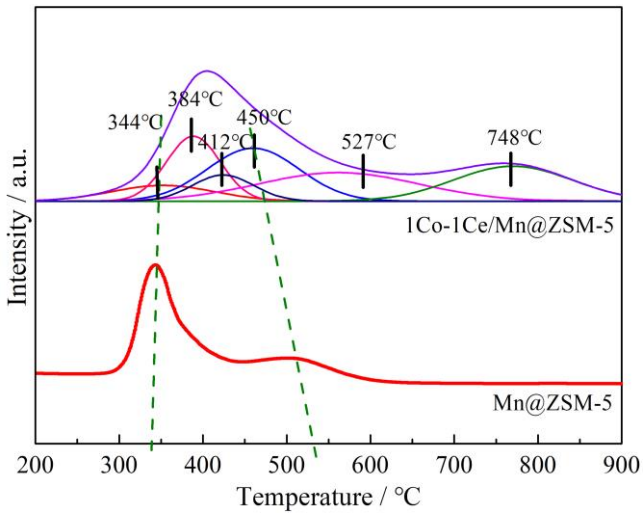

Figure S5. XRD patterns of different catalysts (a) and (b). (─ZSM-5; ─Mn@ZSM-5; ─1Co-1Ce/Mn@ZSM-5).

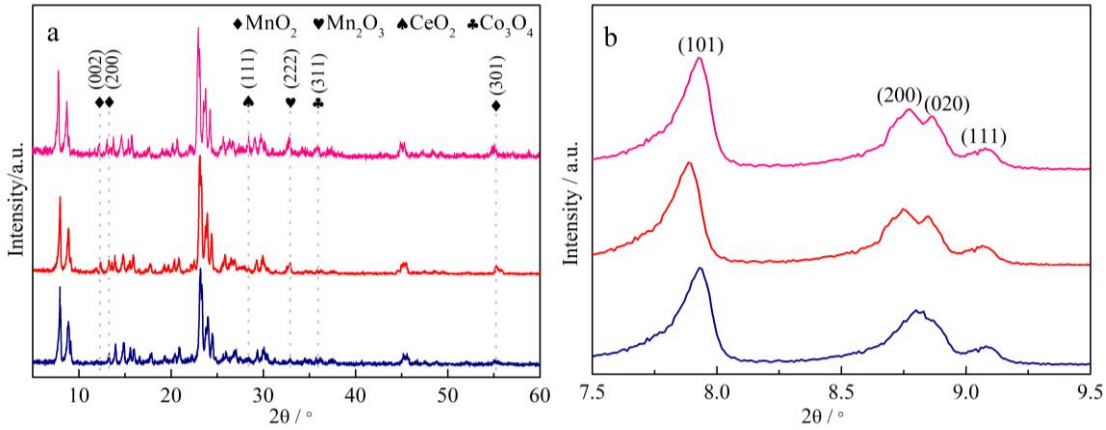

Figure S6. XPS spectra of different catalysts (a: Mn2p; b: Co2p; c: Ce3d; d: O1s).

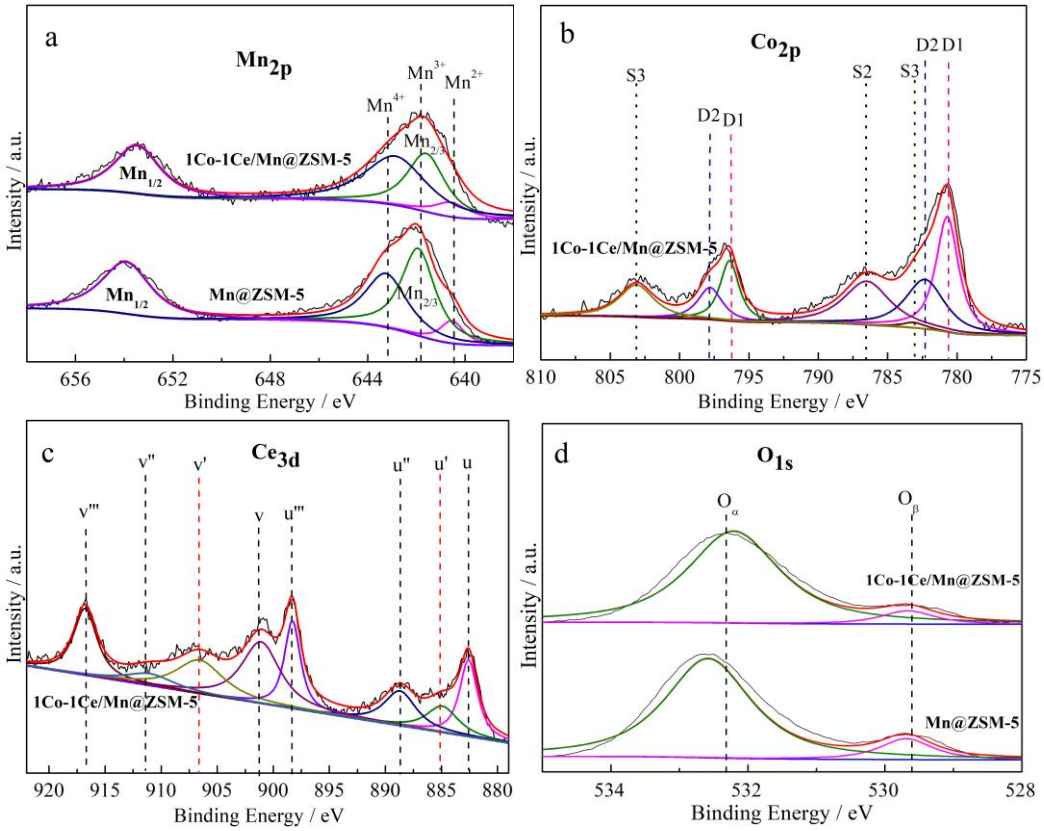

Figure S7. XRD spectra of spent Mn@ZSM-5-SH and 1Co-1Ce/Mn@ZSM-5-SH catalysts (500ppm SO_2 and 5vol% H_2O for 6 h).